SOILS AND FOUNDATIONS Vol. 43, No. 4, 95-106, August 2003
Japanese Geotechnical Society

GRAIN ROTATION VERSUS CONTINUUM ROTATION DURING SHEAR DEFORMATION OF GRANULAR ASSEMBLY

TAKASHI MATSUSHIMA[i], HIDETAKA SAOMOTO[ii], YOSUKE TSUBOKAWA[ii] and YASUO YAMADA[i]

ABSTRACT

The importance of grain rotation during shear deformation has been widely recognized in the mechanics of granular materials, which has led to extensive use of the Cosserat continuum theory in localization problems. Strain gradient theory, which relates the macro deformation gradient to higher-order stresses, is another possibility to overcome the ill-posedness of governing equations. This paper attempts to show an experimental basis for applying strain gradient theory to granular media. LAT (Laser-Aided Tomography), a technique to visualize the interior of 3-*D* granular assembly, is used to detect the grain rotation as well as the continuum rotation. A Discrete Element simulation is also conducted to reinforce the experimental data. It is concluded that the average grain rotation is roughly identical to the continuum rotation, which supports the applicability of rotational gradient theory, a particular case of strain gradient theory from the micro-mechanical point of view.

Key words: Cosserat continuum, DEM (Discrete Element Method), LAT (Laser-Aided Tomography), micromechanics of granular materials, strain gradient theory (**IGC**:D6)

INTRODUCTION

The localization of deformation in softening material has been a major research topic in the field of mechanics. In recent decades, this problem has often been discussed together with the mesh dependency in finite element simulation (Bažant, 1984; de Borst, 1991). To overcome this difficulty, generalized continuum theories (Kröner, 1968) such as the Cosserat continuum theory and the strain gradient theory have been incorporated into the formulation of governing equations (de Borst, 1991; Fleck and Hutchinson, 1997; Chambon et al., 2001; Matsushima et al., 2002), and extensive efforts for application have been investigated for various materials and situations (Murakami et al., 1997; Adachi et al., 1997; Mühlhaus et al., 2001).

Another important issue is the problem of 'size effect'. It is recognized that the bearing capacity of a footing on sand deposit increases with decreasing footing size if the size of sand grains stays unchanged (Tatsuoka et al., 1991). The dynamic stability of rock-fill dam and ballasted railway track are also examples of the size effect. This effect can be expected in every granular structure whose particle size is not sufficiently small in comparison with the whole structure size or, more specifically, with the deformation pattern. Since classical continuum theories cannot deal with this type of micromechanical effects, some researchers have tried to apply the Cosserat continuum theory (Tejchman and Herle, 1999).

The Cosserat continuum contains additional variables for micro rotation, and their gradients (curvatures) are caused by higher-order stresses (couple stresses). The strain gradient theory, on the other hand, does not include an additional variable; macro deformation gradients are related to the higher-order stresses (double stresses). It seems that the Cosserat theory is more suitable for geomaterials than the strain gradient theory, because grain rotation should be essentially independent from macro rotation (continuum rotation). In this way, the Cosserat theory has been studied extensively in the field of particulate mechanics (Mühlhaus and Vardoulakis, 1987; Bardet and Proubet, 1991; Oda and Iwashita, 2000). However, it should be also considered that the Cosserat theory cannot control the mode I localization (pure tension) (de Borst and Mühlhaus, 1992). In that sense, the strain gradient theory is more relevant in the failure analysis of cohesive-frictional materials from the computational point of view.

Physical interpretation of the strain gradient theory is still not clear in comparison with the Cosserat theory. Each theory can be considered as a special case of microstructured continuum theory (Mindlin, 1964; Eringen, 1968), in which all micro deformation gradients are treated as independent variables. In this context, the strain

[i] Associate Professor, Institute of Engineering Mechanics and Systems, University of Tsukuba, 1-1-1 Tennodai, Tsukuba, Ibaraki 305-8573, Japan (tmatsu@kz.tsukuba.ac.jp).
[ii] Graduate Student, Graduate School of Engineering, ditto.
Manuscript was received for review on July 5, 2002.
Written discussions on this paper should be submitted before March 1, 2004 to the Japanese Geotechnical Society, Sugayama Bldg. 4F, Kanda Awaji-cho 2-23, Chiyoda-ku, Tokyo 101-0063, Japan. Upon request the closing date may be extended one month.

gradient theory is understood as a phenomenological simplification, where the micro variables are made identical to the macro variables, and therefore extensive experimental verification is necessary for its application to geomaterials. However, it is not an easy task to observe grain rotation and to compare it quantitatively with continuum rotation in real granular materials. Some researchers have attempted this comparison by Discrete Element Method (Bardet and Proubet, 1991; Choi and Muhlhaus, 1991) or by experiment with circular rods (Calvetti et al., 1997). According to the experiment by Calvetti et al. (1997), the average of grain rotation is in good agreement with continuum rotation when principal stress directions do not rotate. This result suggests that the strain gradient theory is applicable to granular materials from a micromechanical point of view.

This paper attempts further verification on the relationship between grain rotation and continuum rotation in granular materials during shear deformation. The related theories are briefly outlined in the next section to clarify the problem. The main part of this paper is an experiment work using LAT (Laser-Aided Tomography) (Konagai et al., 1992; Matsushima et al., 2002); a visualization technique for 3-D granular assembly. The grain rotation as well as the continuum rotation in the interior of a granular slope model under plane strain deformation are visualized and quantified with the aid of an image analysis technique. The grains used in this experiment are 3-D and have irregular shape as natural sand grains. A supplementary simulation by DEM is also conducted to confirm the experimental results, to make a fruitful discussion and to draw a clearer conclusion.

THEORY OF MICROSTRUCTURED CONTINUUM

General Theory

It is pertinent to review a class of microstructured continuum theory (Mindlin, 1964), from which the strain gradient theory and the Cosserat theory are derived by assuming some mathematical constraints (Chambon et al., 2001). Moreover, it is necessary to make clear how the quantities in this continuum theory can be interpreted with those in granular medium.

The theory begins with the assumption that kinematics of microstructure such as grains, micro cracks and so on cannot be measured in a macroscopic sense, but will contribute to the virtual work of the material during deformation. Global coordinates and displacements (measurable displacement) of a representative volume V are denoted as x_i and u_i, respectively. Then local coordinates x_i' are assumed within V, which moves translationally sticking to the material point but does not rotate. The micro-displacement u_i' in a micro domain is described with these local coordinates and is assumed to be expressed by a linear function of x_i':

$$u_i' = \psi_{ik} x_k' \tag{1}$$

where ψ_{ik} is a constant in a micro domain but a function of x_i, that is:

$$\psi_{ik} = \psi_{ik}(x_i). \tag{2}$$

ψ_{ik} is understood as a gradient of micro displacement within a micro domain. It should be noted that ψ_{ik} is independent from macro displacement gradient du_i/dx_k in this general theory. Now, relative deformation is defined as:

$$\gamma_{ij} \equiv \frac{\partial u_i}{\partial x_j} - \psi_{ij} \tag{3}$$

Additionally, χ_{ijk} is defined as a gradient of ψ_{ik} with respect to x_i:

$$\chi_{ijk} \equiv \frac{\partial \psi_{ij}}{\partial x_k}. \tag{4}$$

where, γ_{ij} and χ_{ijk} are only functions of x_i.

The components of macro strain and rotation under small strain are defined as follows:

$$\varepsilon_{ij} \equiv \frac{1}{2}\left(\frac{\partial u_i}{\partial x_j} + \frac{\partial u_j}{\partial x_i}\right), \tag{5a}$$

$$\omega_{ij} \equiv \frac{1}{2}\left(\frac{\partial u_i}{\partial x_j} - \frac{\partial u_j}{\partial x_i}\right) \tag{5b}$$

Then virtual work is defined as:

$$\delta W = W(\delta\varepsilon_{ij}, \delta\gamma_{ij}, \delta\chi_{ijk})$$

It can be easily recognized that rigid rotation, where γ_{ij} stays at zero, does not affect δW.

On the basis of this assumption, the conjugate stresses are defined as:

$$\sigma_{ji} \equiv \frac{\partial W}{\partial \varepsilon_{ij}} = \sigma_{ij} \tag{6a}$$

$$\tau_{ji} \equiv \frac{\partial W}{\partial \gamma_{ij}} \tag{6b}$$

$$\mu_{jki} \equiv \frac{\partial W}{\partial \chi_{ijk}}. \tag{6c}$$

σ_{ji} is symmetric but this is not the case in general for τ_{ij}. μ_{jki} is called the double stress tensor in this paper, which is a general form of the couple stress tensor in Cosserat continuum.

Accordingly the weak-form equilibrium is described as:

$$\int_V \delta W \, dV = \int_V (\sigma_{ji}\delta\varepsilon_{ij} + \tau_{ji}\delta\gamma_{ij} + \mu_{jki}\delta\chi_{ijk}) dV = \delta P_{ext} \tag{7}$$

where δP_{ext} is an external work caused by body force G_i and boundary forces t_i and T_{ji} which are conjugate with δu_i and $\delta\psi_{ij}$ on kinematically-assigned boundaries. Therefore, it can be described as:

$$\delta P_{ext} = \int_V G_i \delta u_i dV + \int_{\Gamma_u} (t_i \delta u_i + T_{ji}\delta\psi_{ij}) d\Gamma_u. \tag{8}$$

From these equations together with divergence theorem, the strong-form equilibrium is derived as:

$$\frac{\partial(\sigma_{ji} + \tau_{ji})}{\partial x_j} + G_i = 0 \tag{9a}$$

$$\tau_{ji}+\frac{\partial \mu_{jki}}{\partial x_k}=0. \tag{9b}$$

Finally, the corresponding constitutive equations can be expressed as follows:

$$\sigma_{ij}=K^{\varepsilon}_{ijkl}\varepsilon_{kl} \tag{10a}$$

$$\tau_{ij}=K^{\gamma}_{ijkl}\gamma_{kl} \tag{10b}$$

$$\mu_{ijk}=K^{\chi}_{ijklmn}\chi_{lmn}. \tag{10c}$$

Strain Gradient Theory

The strain gradient theory is understood as a particular case of the above-mentioned microstructured continuum with the following constraint:

$$\frac{\partial u_i}{\partial x_k}=\psi_{ik}, \tag{11}$$

which means that the micro displacement gradient ψ_{ik} is identical to the macro displacement gradient. Hence, the governing equations yield:

$$\text{(weak-form)}\quad \int_V \delta W\,dV=\int_V\left(\sigma_{ji}\delta\varepsilon_{ij}+\mu_{jki}\frac{\partial^2\delta u_i}{\partial x_j\partial x_k}\right)dV=\delta P_{ext} \tag{12}$$

$$\text{(strong-form)}\quad \frac{\partial \sigma_{ji}}{\partial x_j}-\frac{\partial^2\mu_{jki}}{\partial x_j\partial x_k}+G_i=0 \tag{13}$$

$$\text{(constitutive equations)}\quad \sigma_{ij}=K^{\varepsilon}_{ijkl}\varepsilon_{kl} \tag{14a}$$

$$\mu_{ijk}=K^{\chi}_{ijklmn}\frac{\partial^2 u_l}{\partial x_m\partial x_n} \tag{14b}$$

It should be noted that no additional kinematic variable is included in the equations and that the double stress tensor is related to the second gradient of displacement.

Cosserat Continuum Theory

The Cosserat theory can also be derived from the microstructured continuum theory by assuming:

$$\psi_{(ij)}=0, \tag{15}$$

where the subscript (ij) denotes the symmetric part of the tensor. $\psi_{(ij)}$ is a micro strain so to speak, and only the micro rotation $\psi_{[ij]}$, where the subscript [ij] denotes the anti-symmetric part, is valid in the Cosserat continuum. Some mathematical derivation leads to the well-known set of equations:

$$\text{(weak-form)}\quad \int_V \delta W\,dV=\int_V\left(\sigma^{M}_{ji}\,\delta e_{ij}+\bar{\mu}_{ji}\delta\left(\frac{\partial\bar{\psi}_i}{\partial x_j}\right)\right)dV=\delta P_{ext} \tag{16}$$

$$\text{(strong-form)}\quad \frac{\partial\sigma^{M}_{ji}}{\partial x_j}+G_i=0 \tag{17a}$$

$$e_{klm}\sigma^{M}_{lm}-\frac{\partial\bar{\mu}_{lk}}{\partial x_l}=0 \tag{17b}$$

$$\text{(constitutive equations)}\quad \sigma^{M}_{ji}=K^{e}_{jikl}e_{kl} \tag{18a}$$

$$\bar{\mu}_{ji}=K^{\bar{\psi}}_{jikl}\frac{\partial\bar{\psi}_k}{\partial x_l} \tag{18b}$$

where

$$\sigma^{M}_{ji}\equiv\sigma_{ji}+\tau_{(ji)}+\tau_{[ji]}, \tag{19a}$$

$$\psi_{[ij]}\equiv e_{ijk}\bar{\psi}_k, \tag{19b}$$

$$\mu_{[jk][i]}=\frac{1}{2}e_{jli}\bar{\mu}_{kl}, \tag{19c}$$

$$e_{ij}\equiv\frac{\partial u_i}{\partial x_j}-e_{ijk}\bar{\psi}_k \tag{19d}$$

where σ^{M}_{ji} denotes measurable stress which is not necessarily symmetric, $\bar{\psi}_i$ denotes Cosserat rotation which is independent from continuum rotation, and $\bar{\mu}_{kl}$ denotes couple stress tensor.

Rotational Gradient Theory

Applying Eq. (15) directly into Eq. (7), we obtain another weak-form for the Cosserat continuum:

$$\text{(weak-form)}\quad \int_V \delta W\,dV=\int_V((\sigma_{ji}+\tau_{(ji)})\delta\varepsilon_{ij}+\tau_{[ji]}\delta(\omega_{ij}-\psi_{[ij]})+\mu_{[j]k[i]}\delta\chi_{[ij]k})dV=\delta P_{ext}$$

where ω_{ij} denotes continuum rotation tensor;

$$\omega_{ij}\equiv\frac{1}{2}\left(\frac{\partial u_i}{\partial x_j}-\frac{\partial u_j}{\partial x_i}\right)$$

Now the term $\tau_{[ji]}\delta(\omega_{ij}-\psi_{[ij]})$ is essentially related to the objective of this paper. $\psi_{[ik]}$ is called micro rotation or Cosserat rotation tensor, which has often been discussed in relation to grain rotation (Muhlhaus and Vardoulakis, 1987; Bardet and Proubet, 1991; Oda and Iwashita, 2000). If this micro rotation (=grain rotation) equals the continuum rotation (macro rotation) in granular medium, the term $\tau_{[ji]}\delta(\omega_{ij}-\psi_{[ij]})$ vanishes and the mathematical framework of the theory is identical to that of the strain gradient theory. This particular case of the strain gradient theory, which we call 'rotational gradient theory', has a big advantage in that no additional micro variable is included in the theory and that only the anti-symmetric part of the strain gradient is incorporated. These features allow us to reduce both kinematic variables and the material constants in the higher-order constitutive equation (Eq. (14b)).

It is worth mentioning that Eqs. (16) to (18) in Cosserat theory can also be used in rotational gradient theory with the following interpretation:

$$\sigma^{M}_{ji}=\sigma_{ji}+\tau_{(ji)},\quad e_{ijk}\bar{\psi}_k=\psi_{[ij]}=\omega_{ij}=e_{ijk}\bar{\omega}_k,\quad \mu_{[jk][i]}=\frac{1}{2}e_{jli}\bar{\mu}_{kl}$$

$$e_{ij}=\frac{1}{2}\left(\frac{\partial u_i}{\partial x_j}+\frac{\partial u_j}{\partial x_i}\right)$$

In this framework, measurable stress σ^{M}_{ji} and the corresponding strain e_{ij} are both symmetric, $\bar{\psi}_i$ equals continu-

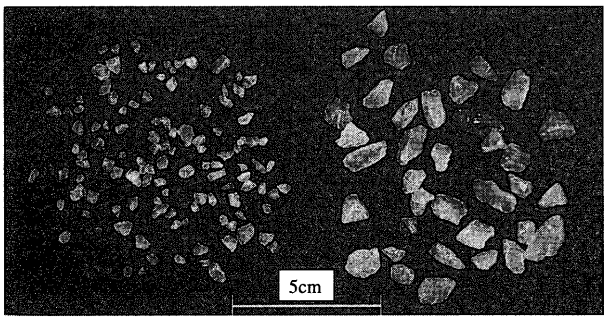

Fig. 1. Grains used in this study (left: $D=2$ mm–5 mm, right $D=5$ mm–10 mm)

Table 1. Material parameters

Glass type	ρ_s (g/cm^3)	Young's modulus (Gpa)	Poisson's ratio
S-BSL7	2.52	78.4	0.205

Table 2. Grain parameters

Grain type	Diameter range	e_{min}	e_{max}
Type 1	2 mm–5 mm	0.670	0.922
Type 2	5 mm–10 mm	0.650	0.935

um rotation ω_{ij}, and couple stress $\bar{\mu}_{kl}$ still remains as a conjugate of ω_{ij}. In other words, couple stress does not always require the grain rotation as independent variables.

EXPERIMENT BY LASER-AIDED TOMOGRAPHY

Outline of LAT Experiment

The visualization technique used in this study is called Laser-Aided Tomography (LAT) developed by Konagai et al. (1992, 1994). Grains used in LAT experiment are produced by crushing and grinding high-quality optical glass blocks. Figure 1 is a photograph of the grains used in this study. Type 1 (Diameter range = 2 mm to 5 mm) and Type 2 (Diameter range = 5 mm to 10 mm) are just sieved apart from the original grains which were ground for 6 hours by a ball mill after crushing. The fundamental properties of the glass itself and grains are listed in Tables 1 and 2, respectively.

In LAT experiment, the grains must be submerged in liquid which has exactly the same refractive index as the glass. In this condition, glass grains are invisible in the liquid. A laser light sheet is then passed through the specimen, which illuminates the contour of the grains within the optically cut cross section (Fig. 2). Therefore, it becomes possible to observe the grain motion in an arbitrary cross section of 3-D granular specimen. Scanning the model by laser light sheet successively, a 3-D image of every grain can also be obtained (Matsushima et al., 2002).

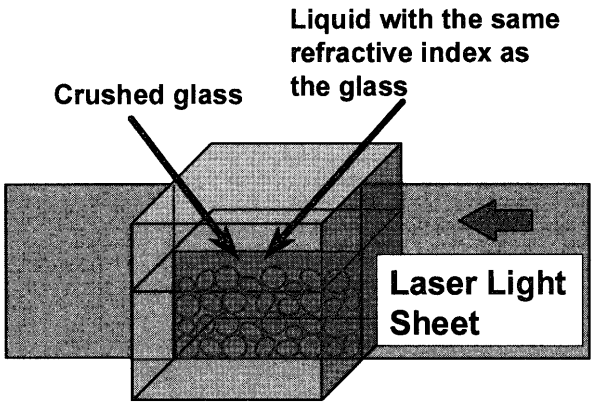

Fig. 2. Diagram of Laser-Aided Tomography

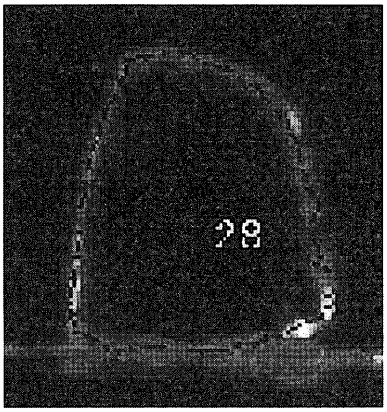

Fig. 3. An example of edge detection

Image Processing Method

In order to quantify each grain location and shape in LAT imageries, some image analyzing technique suitable for LAT is necessary. A semi-automatic graphical users interface (GUI) has been developed for this purpose, which allows for a man-computer interactive operation in which an operator can identify a grain by roughly tracing its contour by a mouse pointer. Then, the computer finds the pixels which has the maximum light intensity among the neighboring pixels (Fig. 3). Once grain contour is digitally detected, the gravity center, area, principal axes of the grain, etc. can be computed straightforwardly.

Experimental Setup

Slope stability tests were conducted in this study. Two types of grains having the following diameters (Type 1: $D=2$–5 mm, Type 2: $D=5$–10 mm, *see* Table 2) are piled up in an acrylic water tank full of the above-mentioned liquid in the same slope configuration illustrated in Fig. 4. In order to make the slope as dense as possible in the liquid, each liquid-pluviated layer of 2 cm thick was compacted by a falling weight. In order to reduce the friction between grains and the walls of the water tank, tempered glass plates are put between them. Then an acrylic footing of 3.3 cm wide was penetrated with the speed of 1.0 mm/min, and the vertical load and displacement were measured during the test.

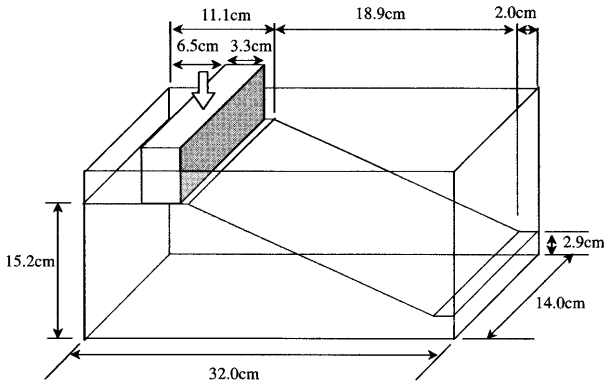

Fig. 4. Experimental setup

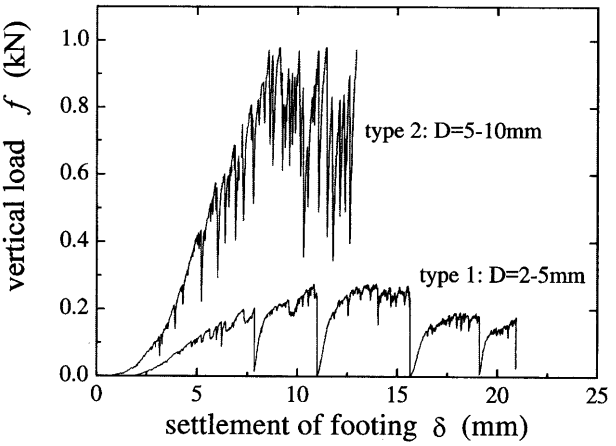

Fig. 5. Load-displacement curve of footing

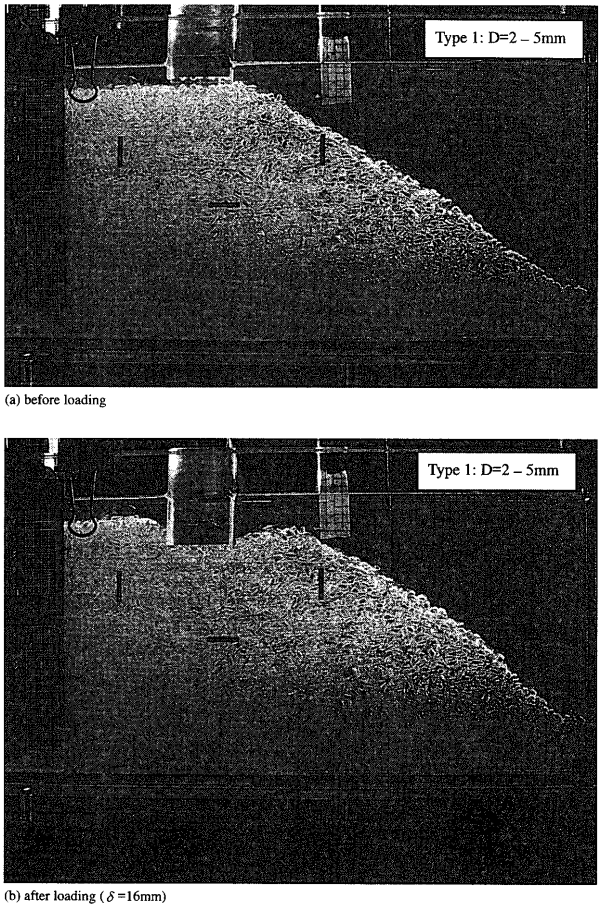

Fig. 6. Deformation of slope by LAT image (Type 1: D = 2–5 mm) (a) before loading and (b) after loading (δ = 16 mm)

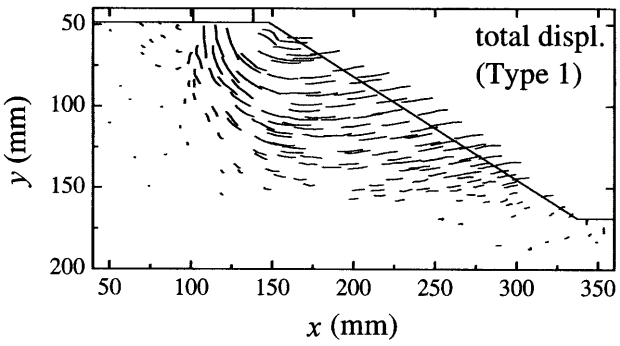

Fig. 7. Translational displacement of grains analyzed from LAT images (Type 1: D = 2–5 mm)

The laser light sheet was passed through the model perpendicularly, and the observed LAT image was photographed by two digital cameras, one for the whole view and the other for a close-up view just beneath the footing. The location of the laser light sheet was fixed at 2.5 cm and 3.5 cm behind the front surface of the model of Type 1 and Type 2, respectively.

Grain Size Effect and Progressive Failure

Figure 5 shows the load-displacement curves of the footing. It is quite clear that Type 2 model (with bigger grains, D = 5–10 mm) exhibits considerably higher strength than Type 1 model. Since maximum and minimum void ratios of Type 1 grains are similar to those of Type 2 grains, grain-shape characteristics may be similar to each other, and accordingly the internal friction angle of the most-densely packed specimen under uniform deformation may not differ much in both models. Therefore, the clear difference of strength shown in Fig. 5 is understood as grain size effect: the effect caused by the ratio between the size of imposed deformation pattern and the grain size. From a viewpoint of the microstructured continuum, when gradient of rotation (macro or micro rotation) is imposed by boundary displacements or forces, microstructural effect (strain gradient effect or Cosserat effect) appears, which makes the material stronger. The magnitude of this effect depends on internal length scale (grain size) involved in the higher-order constitutive equation. Therefore, it is expected that this kind of grain size effect can be well expressed by the microstructured continuum theory.

It should be noted that some sudden drops in load observed in load-displacement curves are mainly caused by the lateral slip of the footing. Since the surface of the footing bottom is not perfectly smooth, the footing moves laterally according to the lateral displacement of

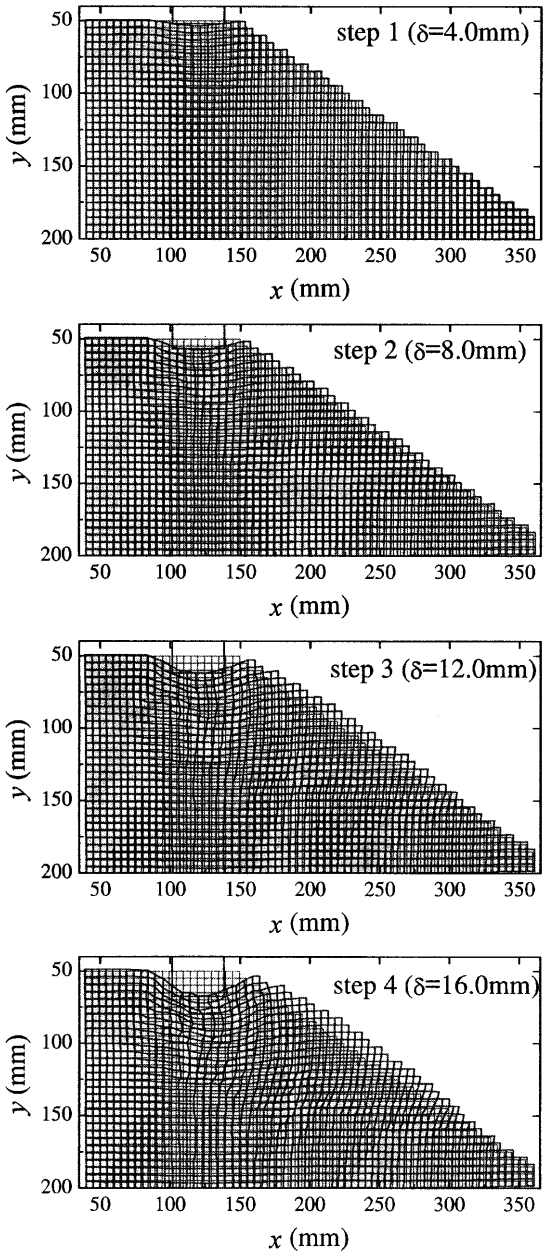

Fig. 8. Deformation patterns computed from grain displacements (Type 1: D=2–5 mm)

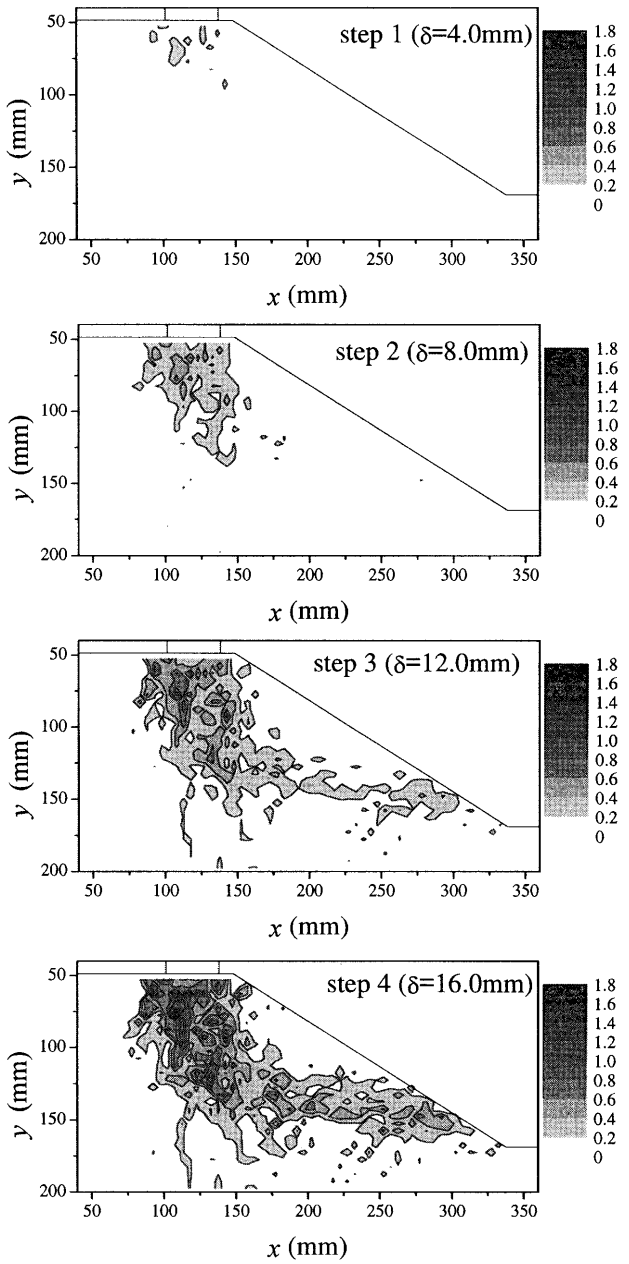

Fig. 9. Maximum shear strain computed from deformation patterns (Type 1: D=2–5 mm)

the granular model. When the friction force reaches a threshold, a slip occurs between the footing and the granular model, which affects the vertical load of the footing.

Another important issue is progressive failure. As the gradient of rotation becomes predominant within the shear zone, the progressive formation of shear zone plays an important role in the bearing capacity of footing. Figure 6 shows the observed LAT images (whole view in type 1 model). Since it is difficult to detect the grain shape with good accuracy from such whole-view photographs, only translational motion of a certain number of grains are detected in this section as shown in Fig. 7. Additionally, the tracked motion is the one within the certain vertical plane sliced by laser light sheet. Therefore, it is not an exact motion of the grains because the grains move and rotate in all six degrees of freedom. However, under the plane strain condition, major translational displacements of the grains can be observed in the plane parallel to the plane strain boundary, and the measured in-plane motion must provide the major deformation pattern. Figure 8 shows the mesh deformation (mesh size = 5 mm by 5 mm) computed from the grain motion by using weighted-average interpolation. For each nodal point, the nearest six grains were used for the interpolation. This number of grains was decided such that the result contains the effect of local deformation to a sufficient extent.

This kind of interpolation is regarded as an averaging process of discrete quantities such as grain motion. Therefore, the resultant deformation is considered as the

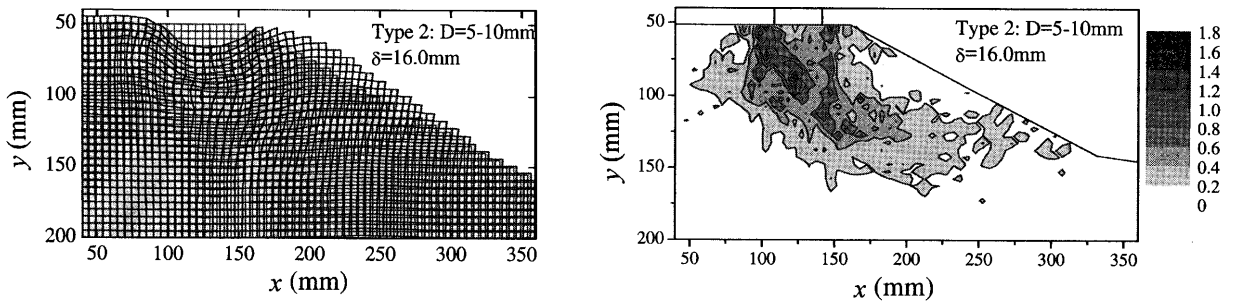

(a) deformation pattern (b) maximum shear strain

Fig. 10. Deformation pattern and maximum shear strain (Type 2: D=5–10 mm)

macro deformation in the context of microstructured continuum theory.

After the interpolation, it is straightforward to compute strain at each mesh from its nodal displacements by linear interpolation. In other words, strain is not directly calculated from the discrete quantity in this study. Figure 9 shows the distribution of maximum shear strain. This figure clearly shows that the strain localization develops progressively. Together with Fig. 5, it can be recognized that the peak strength is reached when the localization zone entirely develops within the model to reach the slope surface.

Figure 10 shows a deformation pattern and a distribution of maximum shear strain in Type 2 model. The settlement of footing is almost the same as that at step 4 in the Type 1 model. When comparing the deformation pattern of Type 2 model with that of Type 1, Type 2 model exhibits significant dilation near the footing. This must be caused by the difference in shear band width between the two models. It is well known that the shear band width is roughly proportional to grain size (Muhlhaus and Vardoulakis, 1987; Yoshida et al., 1994). The maximum shear strain in the Type 2 model shown in Fig. 10(b) also looks widely distributed in comparison with that in the Type 1 model shown in Fig. 9 (step 4). With wider shear zone the total volume change necessarily becomes bigger.

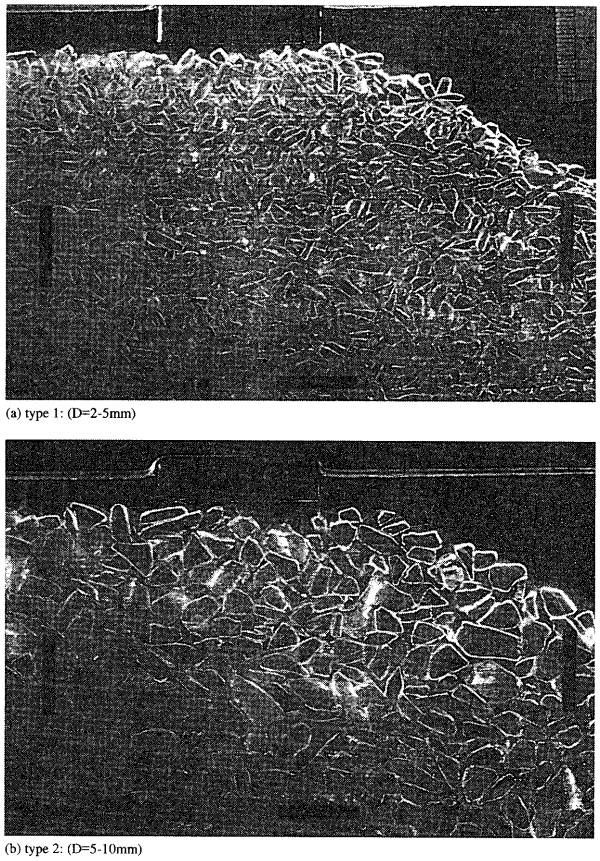

(a) type 1: (D=2-5mm)

(b) type 2: (D=5-10mm)

Fig. 11. Close up view of LAT image (initial state) (a) Type 1: (D=2–5 mm) and (b) Type 2: (D=5–10 mm)

Grain Rotation versus Continuum Rotation

A small rectangular window beneath the footing was chosen as the observation area for grain rotation. Figures 11(a) and (b) show the LAT images of Type 1 and 2 models before loading. The above-mentioned grain edge detection scheme was applied for such images, which yields Fig. 12. In this paper, we discuss only an apparent "in-plane" grain rotation. It is quite certain that grains in the specimen rotate in a three-dimensional way even under plane-strain condition (Matsushima et al., 2000). This rotation makes the in-plane image of the grains gradually change with respect to time. However, according to Fig. 12, most of the grain images do not change much, and the major rotation seems to occur in the plane parallel to the strain-constraint plane due to shear deformation.

In order to compute the in-plane rotation, an image-mapping algorithm shown in Fig. 13 was adopted. Since the rotation of roundish grains is difficult to evaluate, the original result includes a few grains showing unrealistic rotation in the original result. Eliminating such data, Fig. 14 demonstrates the evolution of grain rotation through the loading steps. In the figure, positive values mean counter-clockwise rotation. The grain rotation field within the analyzing area is then calculated by the weighted-average interpolation (Fig. 15). Comparing to Fig. 9, one can easily recognize that the grain rotation is predominant within the localized zone.

Finally Figs. 16(a) and (b) show the relation between the grain rotation, θ_G, and the continuum rotation, θ_C, at

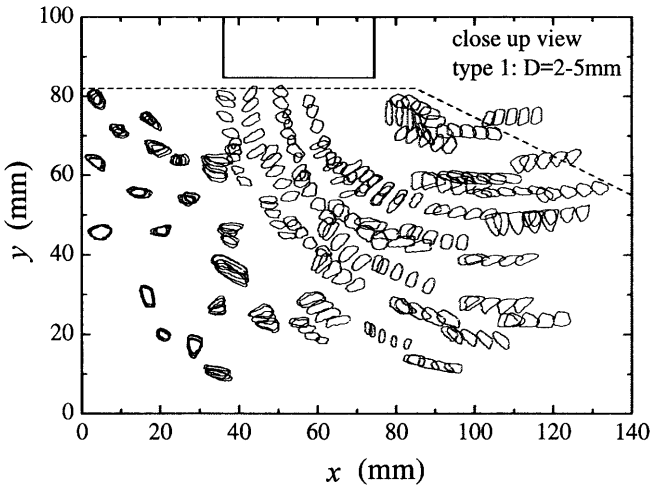

(a) type 1: (D=2-5mm)

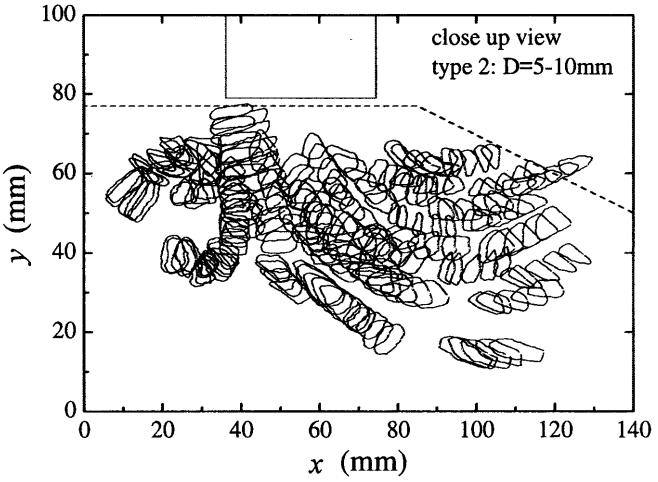

(b) type 2: (D=5-10mm)

Fig. 12. Result of edge detection of the grains (a) Type 1: (D=2-5 mm) and (b) Type 2: (D=5-10 mm)

step 4 for Type 1 and 2 models, respectively. The former is measured at the center of each grain and the latter is computed for the same center from the deformation mesh shown in Fig. 8 by bilinear interpolation. Since the deformation and rotation are far beyond the small strain range, the continuum rotation is calculated on the basis of rigid rotation tensor $\boldsymbol{R}$ (*see* Bardet and Proubet, 1991, for example) as follows:

$$\boldsymbol{R}=\begin{bmatrix} \cos\theta_C & \sin\theta_C \\ -\sin\theta_C & \cos\theta_C \end{bmatrix}=\boldsymbol{V}^{-1}\boldsymbol{F}$$

where $\boldsymbol{V}$ is the left stretch tensor (symmetric) and $\boldsymbol{F}$ is the (macro) deformation gradient. It is worth emphasizing that this continuum rotation is calculated only from the translational motions of the grains and does not include the information of grain rotations.

[1] Select the grains which are clearly detectable throughout the loading steps
[2] Loop for each grain
[3] Loop for each loading step
[4] Compute the gravity center and remove the translational motion from the grain edge data
[5] Rotate the edge data with respect to the gravity center and compare the edge data at the initial configuration. Detect for each edge point the minimum distance from the edge point at the initial configuration.
[6] Compute the summation of the distance for all edge points and determine the rotation angle which gives the minimum summation.
[7] Next loading step (return [3])
[8] Next grain (return [4])

Fig. 13. Algorithm to compute the in-plane rotation of grains

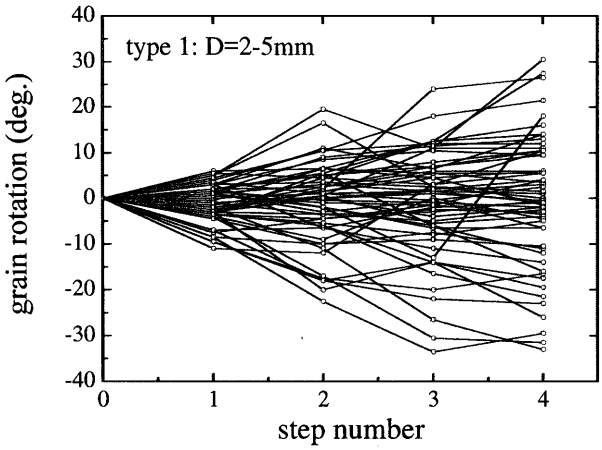

Fig. 14. Evolution of grain rotation (Type 1)

The points in the figures scatter considerably, which is caused by the discrete nature of grain rotations. Our focus should be put on the averaged relation shown as dashed lines in the figures. Roughly speaking, the grain rotation is about the same or a little bigger than the continuum rotation. Therefore, it is suggested that the assumption in the strain gradient theory is roughly acceptable.

NUMERICAL RESULT BY DISCRETE ELEMENT METHOD

In order to further discuss the relation between the grain rotation and the continuum rotation, a series of simple shear simulation by Discrete Element Method were performed. Figure 17 shows the outline of the simulation. Two specimens with circular grains and regular polygonal grains, respectively, are prepared in dense condition. The mean diameter of those grains is 2.0 cm. Periodic boundaries are introduced on both sides of the specimen. Keeping the confining pressure, σ_n, constant ($\sigma_n \approx 0.28$ N/cm), the bottom wall element is moved in a horizontal direction. Accordingly, the specimen is

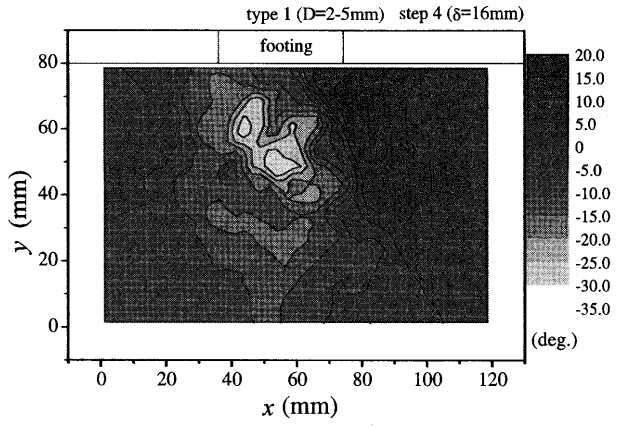

Fig. 15. Distribution of grain rotation

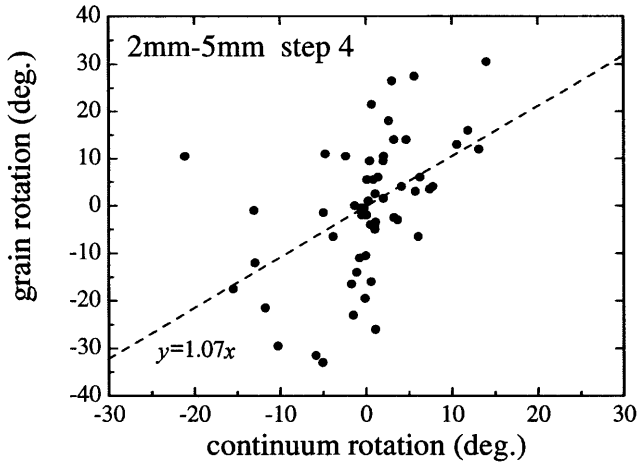

(a) type 1 (D=2-5mm)

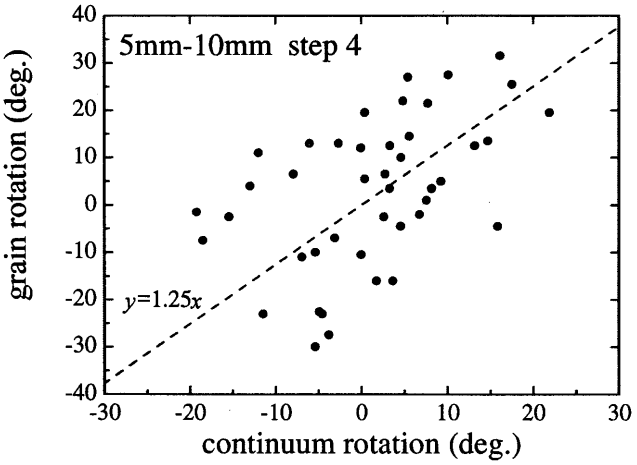

(b) type 2 (D=2-5mm)

Fig. 16. Relation between continuum rotations and grain rotations (step 4)
(a) Type 1: (D=2–5 mm) and (b) Type 2: (D=5–10 mm)

sheared and a level shear band is built up as shown in Fig. 17(b). More detailed information on this series of simulation is described in other papers (Matsushima, 1997; Matsushima and Konagai, 2001).

Since the deformation varies only in y-direction due to the boundary condition, the specimens were divided horizontally into slices by the averaging process (as indicated in Fig. 17(a)). The continuum rotation was computed in the same manner as in LAT experiment for rectangular meshes, but for slices in this case, since it remains unchanged in horizontal direction due to the periodic boundary condition. Grain rotations are simply averaged for each sliced area. The relations between the continuum rotation and the grain rotation for the two specimens are shown in Figs. 18(a) and (b), respectively. The average line indicates that the rotations of both specimens are almost identical to each other. Figures 19(a) and (b) show the distribution of the rotations along the height of the specimens. It is quite clear that the grain rotation is scattered but its average is in good accordance with the continuum rotation. It can be said that all the numerical results support the insights obtained by the experiment.

It is worth noting that the grain rotation is more oscillated in circular grains than in regular polygon grains possibly because the circular grains in contact tend to rotate to an opposite direction to each other like a gear motion, while regular polygon grains behave like a rigid column due to the transmission of the moments at their contacts (Iwashita and Oda, 2000; Matsushima and Konagai, 2001).

SOME COMMENTS

The physical interpretation of the assumption that the grain rotation is identical to the continuum rotation may be shown in Fig. 20. Any macro deformation gradient $\boldsymbol{F}$ can be decomposed by macro stretching $\boldsymbol{V}$ and macro rigid rotation $\boldsymbol{R}$. Under macro rigid rotation of the material, all the grains in the material rotate the same amount. On the other hand, under macro stretching, the grains rotate actively and randomly, but the average of their rotations remains unchanged as illustrated in Fig. 20.

Even though the grain rotation is identical to the continuum rotation, a non-classical term becomes active under the existence of the gradient of continuum rotation. Since grains rotate in accordance with the continuum rotation, the gradient of grain rotation is also induced, which causes additional energy together with the moment at a contact point. In this way, the rotational gradient theory can be reasonably applied to granular material.

Finally, the coincidence between total grain rotation and total continuum rotation breaks when the magnitude of grain rotation exceeds around 45 degrees. This is quite natural if we suppose applying a huge extent of simple shear into granular medium. There is no limitation in grain rotation, while the total continuum rotation cannot

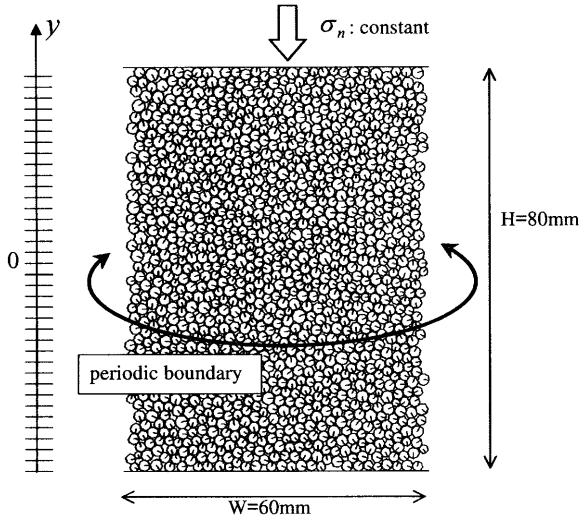

(a) initial configuration

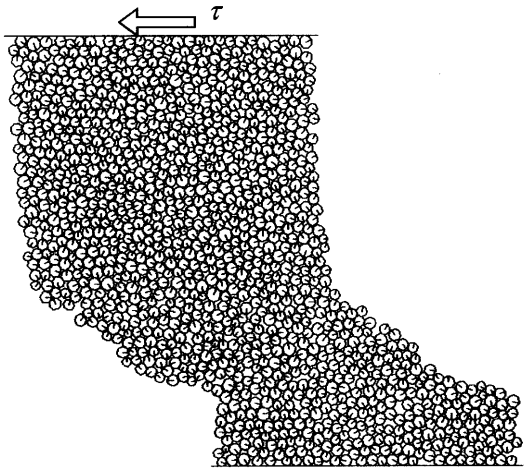

(b) shear strain γ =0.5

Fig. 17. Outline of DEM simple shear simulation (regular polygonal grains: average shape is octagon) (Matsushima and Konagai, 2001) (a) initial configuration and (b) shear strain $\gamma = 0.5$

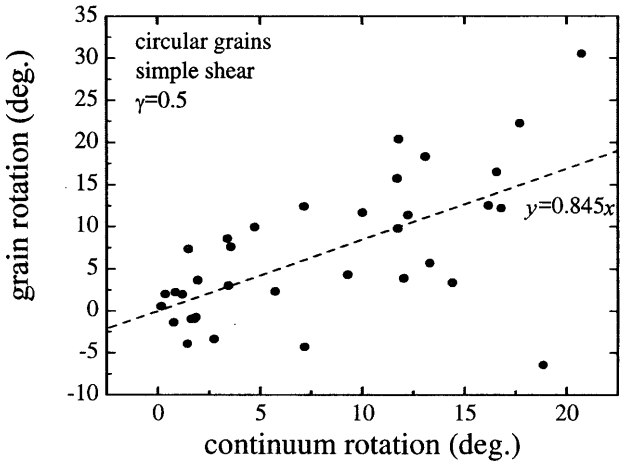

(a) circular grains

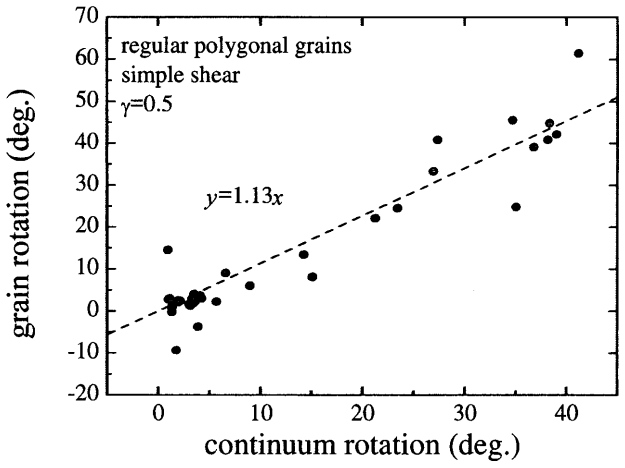

(b) regular polygonal grains

Fig. 18. Relation between continuum rotations and grain rotations in DEM simple shear simulation (a) circular grains and (b) regular polygonal grains

exceed 90 degrees. Therefore, strictly speaking, both rotations should be treated as incremental quantities, continuum spin and granular spin.

CONCLUSION

The relation between the grain rotation and the continuum rotation during the shear deformation of granular medium was studied experimentally and numerically. Both results support the assumption in the rotational gradient theory; a particular case of the strain gradient theory where the above two rotations are identical. The physical interpretation of the rotational gradient theory with respect to granular medium is also presented.

In LAT experiment on slope failure, grain size effect was also discussed together with the progressive failure and the dilatancy behavior of the slope. Such behaviors are tightly related to the reason why non-classical theory is necessary in large deformation problem of granular medium.

Such micromechanical effects have been extensively studied in relation to the internal length that may corresponds to the mean grain size. On the other hand, some researches have focused on the effect of grain shape (Yoshida et al., 1994; Matsushima, 1997; Iwashita and Oda, 2000). Such attempts are necessary to identify the material parameters in higher-order constitutive equation as well as the classical one. The results obtained in this study will also be useful for such future study.

ACKNOWLEDGMENT

Authors gratefully acknowledge Mr. Iidaka of the University of Tsukuba for the preparation of the LAT experiment. The first author is grateful for invaluable discussion on microstructured continuum with Prof. Chambon of Laboratoire 3S, Grenoble. This work was supported in part by a grant-in-aid of Japan Society for the Promotion of Science (No. 13650535).

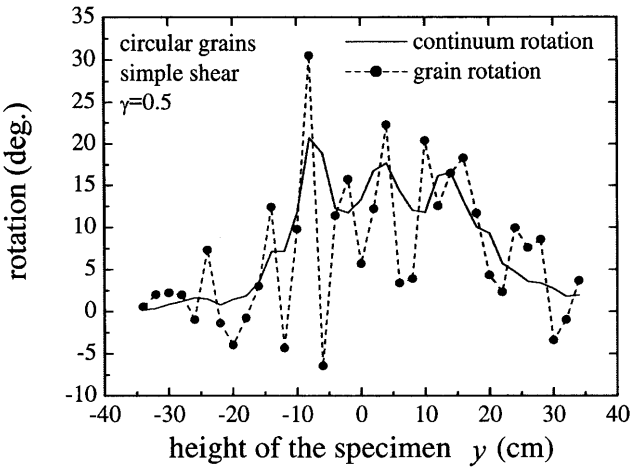

(a) circular grains

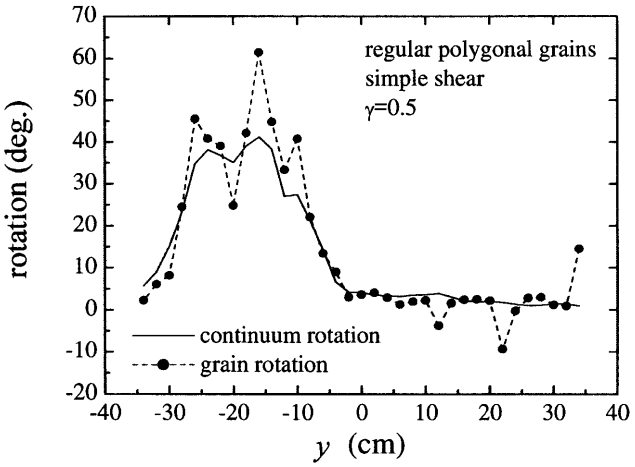

(b) regular polygonal grains

Fig. 19. Distributions of continuum rotations and grain rotations in DEM simple shear simulation
(a) circular grains and (b) regular polygonal grains

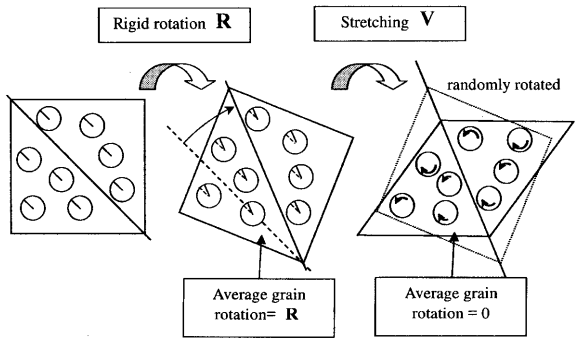

Fig. 20. Physical interpretation of the assumption in strain gradient theory

REFERENCES

1) Adachi, T., Oka, F. and Yashima, A. (1997): Localization and bifircation theory for soils and rocks, *Proc. of the 5th Int. Workshop on Bifurcation and Localisation Theory in Geomechanics*, Balkema.
2) Bardet, J. P. and Proubet, J. (1991): A numerical investigation of the structure of persistent shear bands in granular media, *Géotechnique*, **41** (4), 599-613.
3) Bažant, Z. P. (1984): Imbricate continuum and its variational derivation, *J. Engrg. Mech. Div.*, ASCE, **110** (12), 1693-1712.
4) Calvetti, F., Combe, G. and Lanier, J. (1997): Experimental micromechanical analysis of a 2D granular material: relation between structure evolution and loading path, *Mech. Cohesive-Frictional Materials*, **2**, 121-163.
5) Chambon, R., Caillerie, D. and Matsushima, T. (2001): Plastic continuum with microstructure, Local Second Gradient Theories for Geomaterials: Localization Studies, *Int. J. of Solids and Structures*, **38**, 8503-8527.
6) Choi, S. K. and Muhlhaus, H.-B. (1991): Distinct elements vs Cosserat theory: A comparison for the case of an infinite shear layer, *Computer Methods and Advances in Geomechanics*, (eds. by Beer, Booker and Carter), Balkema, 315-319.
7) de Borst, R. (1991): Simulation of strain localization: A reappraisal of the Cosserat continuum, *Engrg. Computations*, **8**, 317-332.
8) de Borst, R. and Mühlhaus, H.-B. (1992): Gradient-dependent plasticity: formulation and algorithmic aspects, *Int. J. Numer. Meth. Engrg.*, **35**, 521-539.
9) Eringen, A. C. (1968): Mechanics of micromorphic continua, Mechanics of Generalized Continua, *Proc. IUTAM*, Springer-Verlag, 18-35.
10) Fleck, N. A. and Hutchinson, J. W. (1997): Strain gradient plasticity, *Advances in Aapplied Mechanics*, **33**, 295-361.
11) Iwashita, K. and Oda, M. (2000): Micro-formation mechanism of shear banding process based on modified distinct element method, *Powder Technology*, **109**, 192-205.
12) Konagai, K., Tamura, C., Rangelow, P. and Matsushima, T. (1992): Laser-Aided Tomography: A tool for visualization of changes in the fabric of granular assemblage, *Structural Engrg./Earthquake Engrg.*, JSCE, **9** (3), 193s-201s.
13) Konagai, K., Matsushima, T. and Sato, T. (1994): Dependence on frequency of dynamic inter-particle dislocation within a slope, *Structural Engrg./Earthquake Engrg.*, JSCE, **11** (2), 93s-101s.
14) Kröner, E. (1968): Mechanics of generalized continua, *Proc. IUTAM*, Springer-Verlag.
15) Matsushima, T. (1997): Grain-to-grain interaction affecting dynamic deformation of granular slope, *Doctoral Dissertation*, University of Tokyo (in Japanese).
16) Matsushima, T. and Konagai, K. (2001): Grain-shape effect on peak strength of granular materials, Computer Methods and Advances in Geomechanics, *Proc. 10ACMAG*, (eds. by Desai et al.), **1**, 361-366.
17) Matsushima, T., Chambon, R. and Caillerie, D. (2002a): Large strain finite element analysis of a local second gradient model: application to localization, *Int. J. Numer. Meth. Engrg.*, **54**, 499-521.
18) Matsushima, T., Ishii, T. and Konagai, K. (2002b): Observation of grain motion in the interior of a PSC test specimen by Laser-Aided Tomography, *Soils and Foundations*, **42** (5), 27-36.
19) Mindlin, R. D. (1964): Microstructure in linear elasticity, *Arch. Rational Mech. Anal.*, **16**, 51-78.
20) Mühlhaus, H.-B. and Vardoulakis, I. (1987) The thickness of shear band in granular materials, *Géotechnique*, **37** (3), 271-283.
21) Mühlhaus, H.-B., Dyskin, A. and Pasternak, E. (2001): Bifurcation and localisation theory in geomechanics, *Proc. of the 5th Int. Workshop on Bifurcation and Localisation Theory in Geomechanics*, Balkema.
22) Murakami, A., Sakaguchi, H. and Hasegawa, T. (1997): Dislocation, vortex and couple stress in the formation of shear bands under trap-door problems, *Soils and Foundations*, **37** (1), 123-135.

23) Oda, M. and Iwashita, K. (2000): Study on couple stress and shear band development in granular media based on numerical simulation analysis, *Int. J. of Engrg. Science*, **38**, 1713–1740.
24) Tatsuoka, F., Okahara, M., Tanaka, T., Tani, K., Morimoto, T. and Siddiquee, M. S. A. (1991): Progressive failure and particle size effect in bearing capacity of a footing on sand, *Proc. Geotech. Engrg. Congress*, ASCE Geotech. Special Publication (27), 788–802.
25) Tejchman, J. and Herle, I. (1999): A "Class A" prediction of the bearing capacity of plane strain footings on sand, *Soils and Foundations*, **39** (5), 47–60.
26) Yoshida, T., Tatsuoka, F., Siddiquee, M. S. A., Kamegai, Y. and Park, C.-S. (1994): Shear banding in sands observed in plane strain compression, *Proc. Symp. on Localization and Bifurcation Theory for Soils and Rocks* (eds. by Chambon et al.), Balkema, 165–179.